ELSEVIER

Contents lists available at ScienceDirect

Applied Surface Science

journal homepage: www.elsevier.com/locate/apsusc



Full Length Article

Self-organized carbon-rich stripe formation from competitive carbon and aluminium segregation at $Fe_{0.85}Al_{0.15}(110)$ surfaces



Zongbei Dai, Patrizia Borghetti, Younes Mouchaal, Stéphane Chenot, Pascal David, Jacques Jupille, Gregory Cabailh, Rémi Lazzari*

CNRS, Sorbonne Universités, Institut des NanoSciences de Paris, UMR 7588, 4 Place Jussieu, F-75005 Paris, France

ARTICLE INFO

Article history: Received 14 February 2018 Revised 8 March 2018 Accepted 10 March 2018 Available online 12 March 2018

Keywords: Iron aluminide Segregation Random alloy Carbon

ABSTRACT

By combining Scanning Tunnelling Microscopy, Low Energy Electron Diffraction and X-ray Photoelectron Spectroscopy, it was found that the surface of A_2 random alloy $Fe_{0.85}Al_{0.15}(1\,10)$ is significantly influenced by the segregation of aluminium but also of carbon bulk impurities. Below ~ 900 K, carbon segregates in the form of self-organized protruding stripes separated by ~ 5 nm that run along the $[001]_B$ bulk direction and cover up to 34% of the surface. Their C 1s spectroscopic signature that is dominated by graphitic carbon peaks around 900 K. Above this temperature, the surface carbon concentration decays by redissolution in the bulk, whereas an intense aluminium segregation is observed giving rise to a hexagonal superstructure. The present findings is interpreted by a competitive segregation between the two elements.

 $\ensuremath{\text{@}}$ 2018 Elsevier B.V. All rights reserved.

1. Introduction

In response to the environmental imperative of reduction of CO₂ emissions from cars, steel industry develops new generations of highly alloyed light steel grades by using high concentrations of alloying elements such as aluminium [1]. In parallel, iron aluminide is a promising candidate for high temperature structural materials because of its high melting point, excellent formability and good resistance to oxidation [2]. However, during steel processing, complex phenomena of segregation due to alloying elements occur at surfaces or grain boundaries. These latter impact material properties [3,4] such as corrosion resistance and mechanical behaviour; above all, wettability during galvanization becomes a major concern that refers to questions related to metal-oxide interfaces [5–8]. Either as an alloying element or as an impurity, carbon is commonly present on iron and steel surfaces since the range of bulk solubility of carbon in iron is low ($\leq 200 \text{ ppm}$) [9]; the precipitation of carbides (Fe₃C ϵ -cementite or Fe₅C₂ κ -Hägg carbides) in the bulk embrittles steel. Even if a clear tendency towards carbon segregation is predicted by ab initio calculations on Fe(100) and Fe(110) [10,11], there exists during annealing of body-centred Fe single crystal surfaces a complex interplay [12] between the formation of bulk carbide, surface carbidic species, graphite and graphene [13] either upon segregation of bulk

impurities [14-16], dissociation of carbon species [17,18,13] or diffusion of carbon deposited on purpose [19]. On Fe(100) [14-16], in the range of solubility of carbon in iron, the nature of segregated carbon depends on the bulk temperature. Below a dissolution temperature, carbon forms graphite islands while above, a $c(2 \times 2)$ superstructure appears at saturation; the segregation equilibrium can be described by a Langmuir-Mac Lean equation [12] with a segregation enthalpy of $-85 \text{ kJ} \text{ mol}^{-1}$. In near-field microscopy, carbon on Fe(100) appears in the form of lines of nanometer lateral scale arranged in a zig-zag configuration along [110]_R and $[1\overline{1}0]_B$ directions [20]; the self-organization is mediated through interactions between carbon segregated at hollow sites at a coverage of 2/3 with a $c(3\sqrt{2} \times 2)$ superstructure. On Fe(110), carbon is predicted to occupy the long-bridge site [10] although electron diffraction experiments are not so conclusive [21]. However upon exceeding the limit of solubility, a metastable phase of cementite Fe₃C precipitates in the bulk while usually surface graphite forms. But when a third element comes into play, the landscape becomes much more complex. A co-alloying element can induce on carbon segregation synergetic or competitive effects [22,21]. For instance, carbon suffers from site competition from sulfur or silicon on Fe (100) [15,23], a competition governed by diffusivities and segregation enthalphies. Moreover, segregation of carbon in alloys may lead to the stabilization of metastable bulk compounds or even surface compounds that do not have any bulk counterpart such as in the case of FeCrC alloys [12,24].

^{*} Corresponding author.

E-mail address: remi.lazzari@insp.jussieu.fr (R. Lazzari).

Regarding iron aluminide which is the topic of this work, at low carbon contents, the body-centred α phase exists in a disordered random alloy phase (Strukturbericht symbol A2) in the low aluminium concentration corner of the bulk phase diagram [25–27]; at higher aluminium content (\gtrsim 25%-at.), this disordered α phase transforms into ordered states of type B2 and D03. The noticeable solubility for carbon in the A_2 solid phase, that goes up to 1.5% at., has been observed to largely shift the temperatures of the phase transitions between all the polymorphs A₂, B₂, DO₃ [26]. But at higher carbon content, a face-centred cubic solid solution (γ phase) and a ternary intermetallic (κ carbide phase) of defective perovskite structure [27] (E2₁ in the stoichiometric form Fe₃AlC) can be stabilized as well as graphite. If surfaces of iron alumines were shown to be prone to aluminium enrichment for disordered A_2 as well as for ordered B_2 alloys [28–35], the effect of a third element such as carbon was poorly explored up to now. On FeAl(110). density functional calculations predict that adsorption of carbon on FeAl(110) is highly exothermic but endothermic with respect to graphite [11]. Blum et al. demonstrated that the co-segregation of (C, Al, S) at the surface of $Fe_{0.97}Al_{0.03}(100)$ does not take place; the sequence of segregation with temperature $C \rightarrow Al \rightarrow S$ follows the measured segregation enthalpies. While C and S form a full monolayer, Al gives rise only to a $c(2 \times 2)$ reconstruction at this surface [23].

It has been chosen herein to study the segregation at the dense $Fe_{0.85}Al_{0.15}(110)$ surface between 300 and 1100 K as a model system for aluminium alloyed-steel since, in that temperature range, the alloy matrix corresponds to the ferritic A_2 solid solution as in the case of the industrial grades. The effect of an unknown carbon bulk content in the crystal leads to a puzzling segregation behaviour in the form of C-rich stripes. This paper is organized as follows. After a presentation of the methods used (Section 2), the spectroscopic fingerprints and the nature of carbon segregation will be discussed (Section 3.1). Carbon segregation upon annealing in the form of self-organized stripes will be evidenced as well as aluminium surface enrichment by near-field imaging (Section 3.2.1) and electron diffraction (Section 3.2.2).

2. Experimental methods

Experiments have been performed in a ultra-high vacuum set-up composed of a preparation (base pressure $3 \cdot 10^{-10}$ mbar) and a characterization (base pressure $< 1 \cdot 10^{-10}$ mbar) chamber. The disk-shaped single crystal substrate of Fe_{0.85}Al_{0.15} (diameter 6 mm, thickness 2 mm) purchased from Mateck GmbH [36] was cut within 0.1° from the $[1\,10]_B$ orientation and polished down to the lowest achievable roughness. According to the bulk Fe-Al phase diagram [25], the 15% atomic concentration, checked *a posteriori* from the Vegard's law of dependence of lattice parameter versus composition ($a_B = 2.8914$ Å) [37], falls in the body-centred cubic A₂ random alloy structure which is stable up to \sim 1773 K. The (110) bulk truncation parameter leads to a rectangular centred surface unit cell the parameters of which are $a_S = 4.0891$ Å and $b_S = 2.8914$ Å along the $[\overline{1}\,10]_B$ and $[00\,1]_B$ bulk directions, respectively (Fig. 1).

After an initial outgassing of the as-received substrate at $T \geqslant 650$ K, the surface was prepared through cycles of ion sputtering (1 keV, Ar⁺) and annealing (duration 20–40 min) in ultra-high vacuum (pressure $< 1 \cdot 10^{-9}$ mbar) on a dedicated electron bombardment furnace. Temperature (673–1173 K) was determined by an optical pyrometer pointing at the tantalum sample holder and set with an emissivity previously calibrated on a thermocouple spot-welded on it. The annealing did not exceed 1173 K because of potential Al evaporation problems reported on Fe_{0.53}Al_{0.47}(110) above this temperature [29]. Annealed (110) surfaces were characterized (i) by X-ray Photoelectron Spectroscopy (XPS) on a 5-

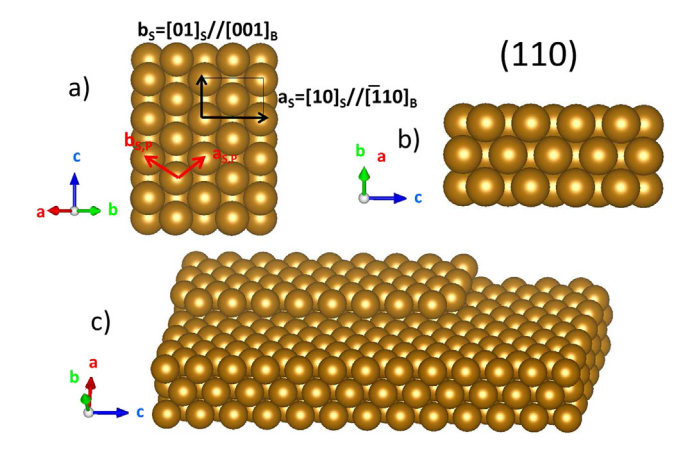


Fig. 1. Ball model of the (110) bulk truncation of body-centred cubic $Fe_{0.85}Al_{0.15}$ random alloy. The brown balls stand for the average atom and the bulk cubic unit cell vectors $(\mathbf{a}_B, \mathbf{b}_B, e_B)$ are shown with coloured arrows. (a) Top view along $[110]_B$. The primitive and rectangular unit cells are shown by red and black arrows, respectively. (b) Side view along $[110]_B$. (c) View in perspective with a monoatomic step. (For interpretation of the references to colour in this figure legend, the reader is referred to the web version of this article.)

channeltron hemispherical analyzer (Omicron EA-125) under non-monochromatic Al-Kα excitation (1486.6 eV), (ii) Low Energy Electron Diffraction (LEED) and (iii) Scanning Tunnelling Microscopy (STM). STM was performed in constant current mode at room temperature (Omicron VT SPM) with a tungsten tip electrochemically etched in a KOH solution. Voltage pulses were used to condition the tip on the clean metallic surface. Gwyddion software [38,39] was used for background subtraction and profile analysis. Due to the very electropositive character of aluminium, contamination from residual background is unavoidable in time during STM measurements. To minimize the effect of ageing in all chemical analysis, photoemission was performed as fast as possible (<30 min) at a pass energy of $E_P = 20$ eV. If not otherwise specified, photoemission spectra are measured at normal emission. The binding energy scale was calibrated on the Ag 3d_{3/2} core level ($E_B = 368.2 \text{ eV}$). After substraction of a Shirley background [40], core level peak decomposition was performed with Doniach-Sunjic asymmetric profiles [41] for metallic components or gaussian functions for others. A Lorentzian broadening of around 0.8 eV due to Al-Kα source was included in peak fitting. Quantification of elements [42-44] was based on the ratios of peak areas after background subtraction and correction (i) for photo-ionisation cross section of the considered core levels [45] and (ii) for analyser transmission function at the corresponding kinetic energies [46]. This corrected signal is proportional to the atomic concentration and exponentially damped up to the vacuum interface through the so-called Inelastic Mean Free Path (IMFP). The integration of the signal depends on the profile of concentration as well on the damping through the crossed layers. Segregation has been modelled in the framework of two schematic approaches, namely a homogeneous mixture and a thin film fully segregated on top of a bulk.

2.1. Homogeneous mixture

If an element A is homogeneously mixed with an element B in a bulk $A_{1-x}B_x$, the atomic concentrations are given by $n_A \sim 1-x$ and $n_B \sim x$. Therefore, the atomic ratio x can be determined from the measured intensities I_A , I_B of given core levels of the elements A and B from:

$$\frac{I_B}{I_A} \frac{T_A \sigma_A}{T_B \sigma_B} = \frac{x}{1 - x} \frac{\lambda_B^{AB}}{\lambda_A^{AB}},\tag{1}$$

Download English Version:

https://daneshyari.com/en/article/7834536

Download Persian Version:

https://daneshyari.com/article/7834536

<u>Daneshyari.com</u>